Influence of Work-Hardening on the Dynamic Stress-Strain Curves of 4340 Steel

BARRY M. BUTCHER* AND JACK R. CANON†
Sandia Corporation, Albuquerque, N. Mex.

The experimentally determined one-dimensional strain dynamic stress-strain curve of R_C54 hardness 4340 steel is shown to be in agreement with the uniaxial strain curve calculated from quasi-static properties. Strain-rate independent elastic-plastic theory including work-hardening was employed in the calculation. The agreement between theory and experiment shows that the stress-strain curve of fully hardened 4340 obtained at low strain rate, which indicates appreciable work-hardening, can be used to predict dynamic behavior. In contrast, the experimental data for R_C15- and R_C32-4340 steel showed strain-rate sensitivity. When these data are analyzed by the same procedure used for the fully hardened steel, a different stress-strain path is obtained for each peak stress level investigated. The results suggest that the observed large increase in flow stress with increase in strain rate is not limited to stress levels around the yield point but persists as long as the strain rate is high.

Introduction

THE determination of Hugoniot equations of state from shock-wave measurements has been reported by many investigators.[1–10] Many of these studies have utilized high explosives to produce shock waves with stresses in excess of 100 kbars.‡ Under these conditions, material rigidity contributes a relatively small amount to the observed stress, so that a strict hydrodynamic model of behavior has been applied with success to the compressive part of the loading cycle. Even at these stress levels, however, rigidity must be considered during unloading to accurately describe the attenuation of a stress pulse as it moves through the material.[11, 12]

At stress levels of the same order of magnitude as the yield stress of the material, the effect of rigidity contributes significantly to all parts of the dynamic stress-strain curve. Fowles[8] has analyzed the dynamic behavior of 2024 aluminum, in the precipitation hardened and annealed conditions, in this stress range by simple elastic-plastic theory. His results show that, within his experimental error, the plastic part of the experimentally determined dynamic stress-strain curve is offset from the hydrostat by $\frac{2}{3}Y_0$, where Y_0 is the static yield strength of the material. Similar results have been obtained for 6061-T6 aluminum by Lundergan and Herrmann.[9] Work-hardening is not observed in either investigation because the flow stress Y of these alloys does not increase markedly with increase in strain; consequently, the experimentally determined stress-strain curves nearly parallel the hydrostats. In contrast, if a material exhibits pronounced work-hardening at small strains, the increase in flow stress Y must be reflected as an increasingly large offset of $\frac{2}{3}Y$ from the hydrostat for increasing strain.

This paper describes the experimental determination of the dynamic stress-strain curve of fully hardened 4340 steel, which exhibits considerable work-hardening in the strain range investigated. The curve is compared with the experimentally determined dynamic stress-strain curves of two softer conditions of 4340 steel which exhibit negligible work-hardening. A comparison is also made between the experimentally determined dynamic stress-strain curves and dynamic curves predicted from the quasi-static properties of 4340. Of particular interest is the accuracy with which the plastic portion of the dynamic curve can be predicted from the results of a quasi-static (strain rates 10 to 10^{-3} in./in./sec) one-dimensional compressive stress test.

The possibility of a correlation between static and dynamic behavior assumes that the increase in flow stress with increased strain rate may be neglected (is of the order of the experimental error), or that the state of stress in the material is measured under the condition of low strain rate. Recent precise measurements by Barker, Lundergan, and Herrmann[13] show that strain-rate effects do exist in 6061-T6 aluminum, a material that previously was thought to be "strain-rate independent." These effects were previously undetected because of the error in the measurement of dynamic response and the method of analysis of the resulting data. This suggests that, for many applications in which a state of one-dimensional strain exists, the precision of the work may not warrant inclusion of strain-rate effects.

Experimental Method and Analysis

The experimental work of this investigation concerned the generation of peak stresses from 10 to 55 kbar in 4340 steel of varying hardnesses. The steel was loaded symmetrically by impacting a flat target plate of uniform thickness with a flat projectile of the same material. Details of the air gun used to accelerate the projectiles to impact velocity are described elsewhere.[9] The stress range corresponds to projectile velocities of 100 to 1000 fps.

The 4340 steel was originally in the form of $6\frac{1}{2}$-in.-diam bar stock. This was cut into $\frac{1}{2}$-in.-thick plates, some of which were reduced to 4 in. in diameter for use as projectile face plates. All plates were then heat treated according to the procedures of Table 1.

After heat treatment several $1\frac{1}{2}$-in. by $\frac{1}{2}$-in.-diam uniaxial compression specimens were ground to shape for quasi-static stress-strain determinations. The results of these tests are shown in Fig. 1. The remaining plates were then parallel ground and lapped flat enough to assure contact of all points of the impact surface within 0.01 μsec. The flatness tolerance is therefore directly related to the proposed projectile velocity and ranges from 12- $\times 10^{-6}$-in. deviation from plane over a 4-in.-diam area for a projectile velocity of 100 fps to ten times that for 1000 fps. The flatness was determined by an optical flat using a monochromatic light source.

Received February 28, 1964; revision received July 6, 1964. This work was supported by the U. S. Atomic Energy Commission.

* Staff Member.

† Staff Member; now Graduate Student, University of Illinois.

‡ 1 kbar = 14,504 psi; compressive stress and strain are taken as positive.

The projectile velocity, tilt, and free surface motion (see Fig. 2) were determined in the plate impact experiments. Tilt is defined as the angle between the face of the projectile and the impact surface of the target just prior to impact. If a perfect impact is not achieved, points on the free surface of the target opposite to points of first contact of impact begin to move first. A corresponding "tilt" in the free surface motion then occurs. Data obtained from different regions of the free surface must then be corrected for this effect before analysis is possible. The tilt in these experiments was always less than 0.05°. All observations of free surface motion were made prior to the arrival of the effects caused by the finite lateral geometry of the projectile, so that a state of one-dimensional strain existed with the principal stress parallel (σ_x) and perpendicular (σ_y, σ_z) to the direction of wave propagation ($\epsilon_y = \epsilon_z = 0$), and from symmetry $\sigma_y = \sigma_z$.

The instrumentation went through three states of refinement during the course of the investigation. The first procedure utilized a circumferential array of eight pins protruding at various lengths from the impact surface to measure tilt and projectile velocity. Electrical contact of these with the moving projectile were observed on an oscilloscope, and the motion of the projectile was deduced from the recorded trace. Similarly, an array of pins set various distances from the free surface were used to determine the distance-time history of the free surface by electrical contact time recordings. The pin settings were not close enough, however, to define the transition between the portions of the free surface motion due to the elastic and plastic parts of the incident wave; consequently, the data points defined two straight lines within experimental error. The first straight line segment was extrapolated to zero to get the arrival time of the elastic wave, and its intersection with the second line segment was taken as the arrival of the plastic wave. This information, the slope of the first line segment, and the projectile velocity measurement permitted calculation of the peak stress and strain in the material from the Hugoniot relations.[3]

The second measurement technique retained the eight pin array for the projectile velocity and tilt determinations. The innovation was a slant wire resistor for monitoring the free surface motion. This is a fine high-resistance wire, with a voltage across it, which is placed at a small angle to the free surface and progressively shorted out during the motion of the surface. The angle is small enough to assure that the velocity of the closeout point on the wire is supersonic so that the propagation of disturbances along the wire into portions that have not yet closed out does not occur. The change in voltage across the wire is recorded during closeout as a function of time and is then reduced to a distance-time history and corrected for tilt.

The present technique[14] uses the slant wire to observe the free surface motion. A schematic of the experimental setup is shown in Fig. 2. The projectile velocity is measured to $\pm 0.3\%$ by determining the closure times of two adjacent pins of different lengths which project from the impact surface. The tilt is determined by four electrically isolated pins that are mounted in the target so that their tips are flush with the impact surface. This greatly increases the accuracy of their positioning and permits the use of very fast sweep speeds to record the closeout times. From this information, the angle between the projectile face and the target surface at impact may be calculated. The slant wire data are then corrected accordingly.

Table 1 Specimen heat-treatment procedures

Hardness	Heat treatment
Rc15	Packed in cast-iron chips, heated to 1450°F, and furnace cooled
Rc32	Heated in a salt bath to 1525°F, oil quenched, and reheated to 1050°F for 2 hr
Rc54	Heated in a salt bath to 1525°F and oil quenched

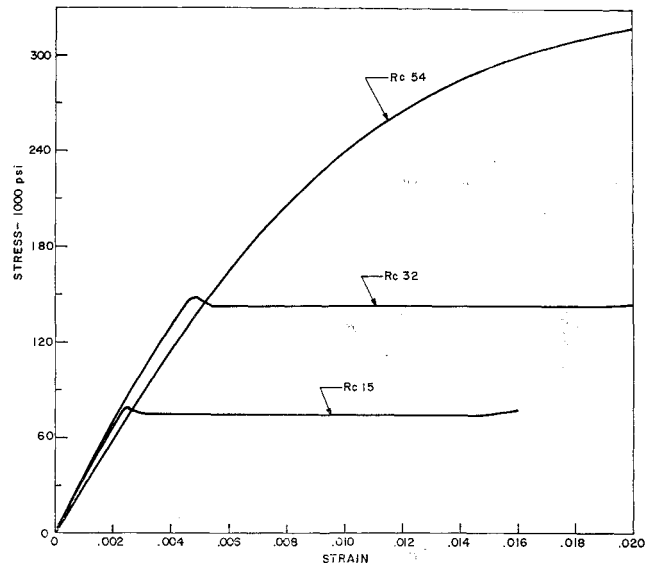

Fig. 1 Quasi-static stress-strain curves (one-dimensional stress) for 4340 steel.

In the experiments in which the slant wires were used, three wires were mounted on each target. The final free surface displacement trace used for the analysis was a composite of the traces from all three wires. This was divided into as many straight line segments as necessary to give a good approximation of the curve. In most cases, four line segments were sufficient. An approximate dynamic stress-strain curve was then calculated[15, 16] by estimating the shock velocities from the segment intersections (these define the time of arrival of each incremental stress pulse) and the material velocity changes from the slopes of adjacent segments. The approximation that the particle velocity change Δu is one-half the change in free surface velocity is generally made. The change in stress associated with each segment was then estimated as

$$\Delta\sigma_x = \rho_0 U_s \Delta u$$

where ρ_0 was taken as the initial density to facilitate calculation. The slope of the stress-strain curve associated with this increment was approximated by

$$\Delta\sigma_x / \Delta\epsilon_x = \rho_0 U_s^2$$

Starting with the first shock velocity-particle velocity pair, then, the complete dynamic stress-strain curve was constructed on the assumption of strain-rate independence. For some engineering calculations at low-stress levels this result is sufficient.

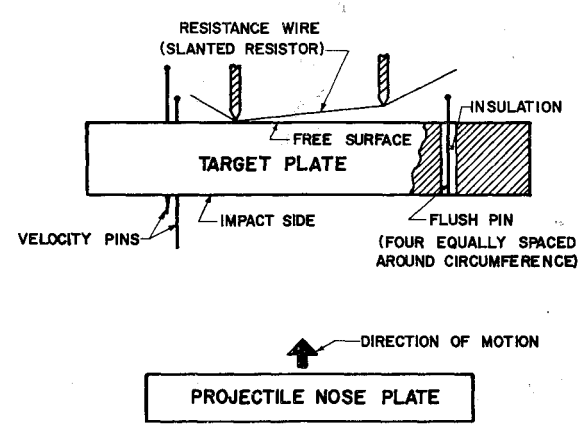

Fig. 2 Schematic diagram of the target instrumentation.

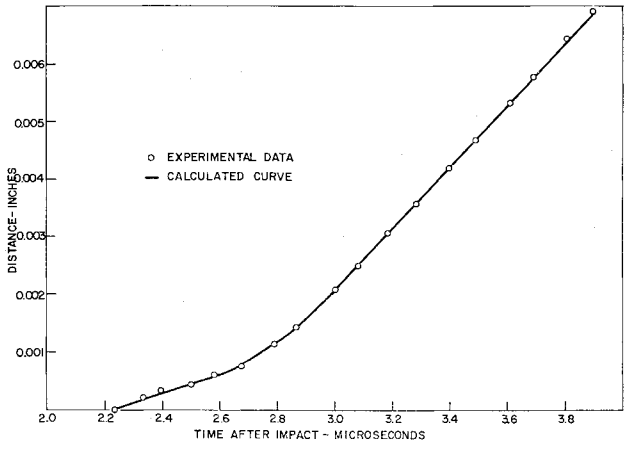

Fig. 3 Free surface distance-time plot for shot 26.

A refinement of this calculation is necessary, however, if the fine details of the dynamic stress-strain curve are to be deduced. The principle objections to the foregoing procedure are that change in density has not been considered, the particle velocity has been approximated, and the unloading by elastic rarefaction waves of the plastic part of the stress wave interacting with the free surface has been neglected. The latter occurs because of the faster propagation velocity of an elastic wave. The elastic wave reaches the free surface first and is reflected as a rarefaction wave moving back into the target. When this pulse meets oncoming plastic waves, the interaction is the same as the transmission and reflection of pulses at a boundary between two slightly dissimilar materials since the densities on each side of the interface are different. Consequently each interaction will have an effect on the free surface motion as the products of these interactions reach the free surface.

In principle, all these calculational refinements may be done by hand, but in practice, this is prohibitively tedious. Instead, the forementioned stress-strain curve estimate was used as the input to a computer program in which the method of characteristics and elastic-plastic strain-rate-independent theory were used to calculate the theoretical free surface motion.[17] A 1604 CDC computer was used. The program determined all shock interactions with free surfaces and other shock waves and subsequently gave a complete stress-strain history for any desired point in the target or projectile. The calculated free surface motion was then compared with the experimental curve, and the dynamic stress-strain curve was altered, if necessary, to improve the agreement. An example of the final result is shown in Fig. 3.§ Numerical results are summarized in Table 2.

Two aspects of the foregoing procedure merit further discussion. The first concerns the assumed path for unloading from the maximum compressive stress produced in the target. In this analysis, the stress-strain curve is taken to be antisymmetric with respect to the strain axis. If a Bauschinger effect is absent,[16] unloading is completely elastic except for the highest stress states of the R_C15, R_C32, and R_C54 steel. Consequently, there is a minimum of work-hardening during the release of the compressive stress. There is no simple way currently available for predicting the change in flow stress with strain after the reverse yield stress is reached. The error introduced by neglecting this, as well as a Bauschinger effect, is estimated to be small. This assertion is based on a series of calculations with the forementioned program in which small perturbations in the unloading path, such as might be expected due to these effects, were assumed and the free surface motion calculated. No significant change in the free surface motion was observed.

§ The experimental data are discrete points that were taken from the continuous voltage trace of the slant wire and then corrected for tilt and transformed to distance-time coordinates by computer.

Table 2 Dynamic stress-strain coordinates for the stress-strain curves of 4340 steel[a]

Hardness	Shot	Stress-kbar/strain			
Rc15	21	19.1	37.4	49.5	57.4
		0.0069	0.0165	0.0239	0.0295
	26	16.8	23.2	34.2	40.8
		0.0062	0.0095	0.0161	0.0211
Rc32	13	19.6	24.7	43.2	56.7
		0.0076	0.0100	0.0205	0.0293
	22	20.3	28.4	54.9	58.8
		0.0073	0.0112	0.0259	0.0287
	25	15.8	21.6	33.5	38.2
		0.0059	0.0085	0.0150	0.0182
	27	13.6	...	...	...
		0.0051	...	...	...
Rc54	12	24.0	35.7	44.7	...
		0.0089	0.0137	0.0180	...
	15	14.3	36.3	47.3	57.0
		0.0055	0.0142	0.0190	0.0237
	16	21.4	...	...	...
		0.008	...	...	...
	17	27.3	27.7	...	...
		0.0104	0.0107	...	...
	18	26.7	31.8	...	...
		0.0100	0.0122	...	...
	19	31.0	52.9	61.9	...
		0.0119	0.0214	0.0264	...

[a] The stress-strain curve is approximated by connecting the coordinates by straight lines.

The second observation is that an error in the measurement of the final surface velocity, when converted to material velocity, causes data points to move along the dynamic stress-strain curve rather than parallel to the stress axis. This is fortuitous since the free surface velocity cannot be measured with the precision of the other measurements. It is most significant that, at high stress levels where changes in stress and strain due to error are greatest, the slope of the stress-strain curve varies slowly. This means that a large error in particle velocity is reflected as a much smaller error in the determination of the stress-strain curve.

In order to compare the experimentally determined curves with those predicted from the quasi-static properties of the material, the state of stress of the material in one-dimensional strain must be specified. This has been developed in general form elsewhere,[8, 15, 16] so only the simplest approach will be reviewed. The principal assumptions in the theory are that 1) there is no volume change due to plastic flow, 2) the flow stress is dependent only on the amount of plastic work done, and 3) a yield criterion of

$$\sigma_x - \sigma_y = Y(W_p) \tag{1}$$

is used.¶

To obtain the functional relation between stress and strain in one-dimensional strain, the strain is first separated into elastic and plastic components:

$$\epsilon_x = \epsilon_x{}^e + \epsilon_y{}^p$$
$$\epsilon_y = \epsilon_z = 0 \qquad \epsilon_y{}^e = -\epsilon_y{}^p \tag{2}$$

The elastic strains in the principle stress orientation ($\sigma_y = \sigma_z$) are then given by

$$\epsilon_x{}^e = (\sigma_x/E) - 2\nu(\sigma_y/E)$$
$$\epsilon_y{}^e = (\sigma_y/E)(1 - \nu) - \nu(\sigma_x/E) \tag{3}$$

¶ Both the Von Mises and Tresca yield criteria take this form for the one-dimensional strain experiments described here.

where E is Young's modulus and ν is Poisson's ratio. At the yield point defined by Eq. (1), plastic deformation begins. The assumption that there is no volume change due to plastic flow requires that

$$\epsilon_x^p + 2\epsilon_y^p = 0 \tag{4}$$

so that combining Eqs. (1–4), the relation between stress and strain above the elastic limit (yield point) is determined to be

$$\sigma_x = \sigma + \tfrac{2}{3}Y(W_p) \tag{5}$$

where

$$\sigma = K\epsilon_x \tag{6}$$

In these equations, σ is the spherical or hydrostatic stress component,** K is the bulk modulus, and the deviatoric stress component $\frac{2}{3}Y(W_p)$ indicates that the flow stress is a function of the plastic work.

In order to apply Eq. (5) to a specific problem, $Y(W_p)$ must be determined. This is most easily accomplished by a one-dimensional stress compression test that must then be related to the one-dimensional strain state through the plastic work.

In one-dimensional stress, the amount of plastic work associated with a change in plastic strain $d\alpha_x^p$ is

$$dW_p = Y\, d\alpha_x^p \tag{7}$$

For one-dimensional strain the plastic work is given by

$$dW_p = \sigma_x d\epsilon_x^p + 2\sigma_y d\epsilon_y^p \tag{8}$$

which, using Eqs. (1) and (2), reduces to

$$dW_p = Yd\epsilon_x^p \tag{9}$$

The transformation between one-dimensional stress and one-dimensional strain is therefore determined by equating equal amounts of plastic work:

$$d\alpha_x^p = d\epsilon_x^p \tag{10}$$

which may be written in slightly more useful form by integrating both sides and then expressing the result in terms of the total strains:

$$\epsilon_x = \tfrac{3}{2}\alpha_x - (Y/6K) \tag{11}$$

The last term is due to the elastic strain components that must be subtracted from the total strain to give the plastic strain.

A general procedure for calculating the dynamic stress-strain curve in one-dimensional strain from a quasi-static one-dimensional stress curve (or from a dynamic one-dimensional stress curve if it is available) is to first choose a point (Y, α_x) on the latter. Using these, σ_x and ϵ_x may be calculated from the equations and specification of K. This process is then repeated until the dynamic stress-strain curve is sufficiently defined. The state of one-dimensional strain may be interpreted to be a one-dimensional stress test under a varying hydrostatic stress condition sufficient to assure no change in lateral dimensions of the specimen.

Since both the compression curve and the compressibility are obtained under conditions of nearly constant temperature, they must be corrected to the thermodynamic conditions of the dynamic stress-strain curve, or conversely. If the energy associated with plastic deformation may be neglected (that is, the material is essentially under hydrostatic pressure), the correction is easily made.[1, 2] However, the flow stresses of the materials under investigation are large, and this approximation cannot be used. Instead, the close proximity of the dynamic stress-strain curve to an adiabat justifies correcting the static data to adiabatic conditions.[9] This significantly changes the compressibility, but the change in the elastic modulus is negligible.

Bridgman's hydrostatic data for fully hardened steel containing 1.1% carbon[18] were used in calculating dynamic stress-strain curves (one-dimensional strain) for all three hardesses of 4340. Although Bridgman's steel was undoubtedly somewhat harder than fully hardened 4340, its compressibility should be more representative than that for softer steels with only small amounts of impurities. For comparison, the compressibility of 1.1% carbon steel is greater by about 2% than the compressibility of American Ingot iron, single crystal iron, and stainless-steel H26, and less than that of stainless-steel H29 by about 2%. This, along with the small effect composition and hardess has on the elastic moduli of steels, suggests that the error in using 1.1% carbon steel values for R_C15- and R_C32-4340 steel cannot be great. Since Bridgman's data are only to 30 kbar, his compressibility function was used to extrapolate to higher pressures. It is expected, therefore, that the error in calculating the highest stress states will be greater than for the lower states.

Discussion

The results of computer calculations for experiments on R_C54-4340 steel using the present experimental technique are shown in Fig. 4. These results represent what is believed to be the present optimum in experimentation and are therefore considered most accurate. Since each experiment yields a complete stress-strain curve, these curves would be expected to fall on top of one another if the approximation that stress is a function of strain only is valid. This would result in the existence of a single unique composite curve defining the relation of stress to strain at all stress levels. Within the limits of experimental error and the errors inherent in the analysis, this is observed for R_C54 steel.

The stress-strain curve calculated from quasi-static compression data has been superimposed on the R_C54 experimental curves in Fig. 4. Again, the difference between predicted and measured results may well be due to the approximations of the analysis and is therefore not considered significant. The close agreement suggests that the dynamic stress-strain curve can be predicted with considerable ac-

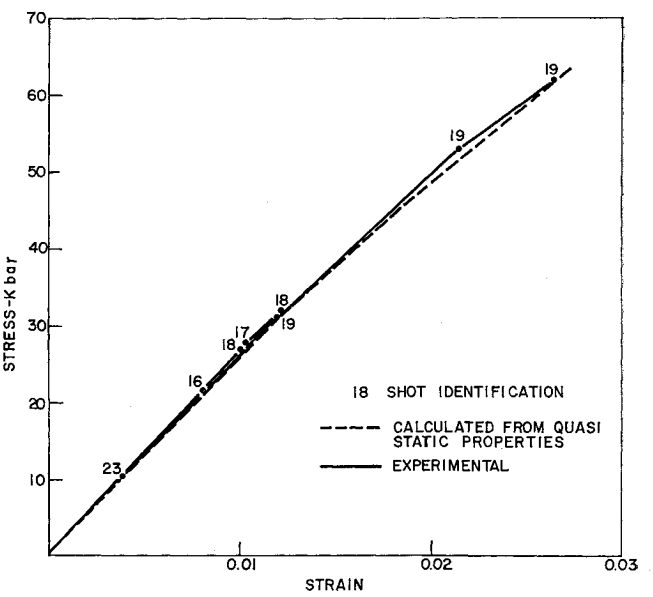

Fig. 4 Dynamic stress-strain curves of R_C54 4340 steel.

** Under the one-dimensional strain condition, $d\epsilon_x = dV/V = dl/l$, where V is the volume of an element and l is its length in the direction of propagation. The strains observed in these experiments were so small that finite strain analysis is unnecessary; natural strain was suitably approximated by nominal or engineering strain.

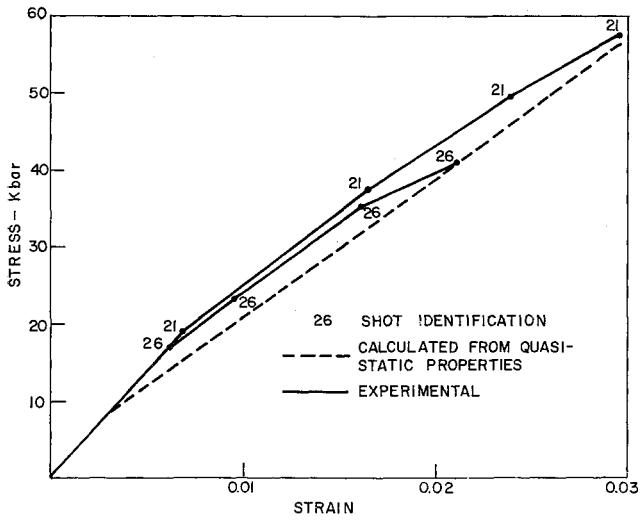

Fig. 5 Dynamic stress-strain curves of R_c15 4340 steel.

curacy from the static properties of this fully hardened 4340 steel.

The results of computer calculations for experiments on R_c15-4340 steel using the present experimental technique are shown in Fig. 5. These differ significantly from the R_c54 curves in that a different curve is observed for each terminal stress state,†† and each curve lies significantly above the curve calculated from quasi-static results. This is, of course, further evidence of the well-known increase in initial flow stress with increase in strain rate observed in steels by Jones, et al.[19] and Taylor and Rice.[7] In addition, however, the offset ($\frac{2}{3}Y$) shows that this increase in flow stress is not confined to the initial portion of the stress front preceding the yield point but is observed in all parts of the stress wave where the strain rate is high. The experimental technique here was not precise enough to observe the dynamic upper yield point of this steel.

The dynamic stress-strain curves in Fig. 5 for R_c15-4340 were obtained using strain-rate-independent elastic-plastic theory. Each portion of the curves therefore represents some

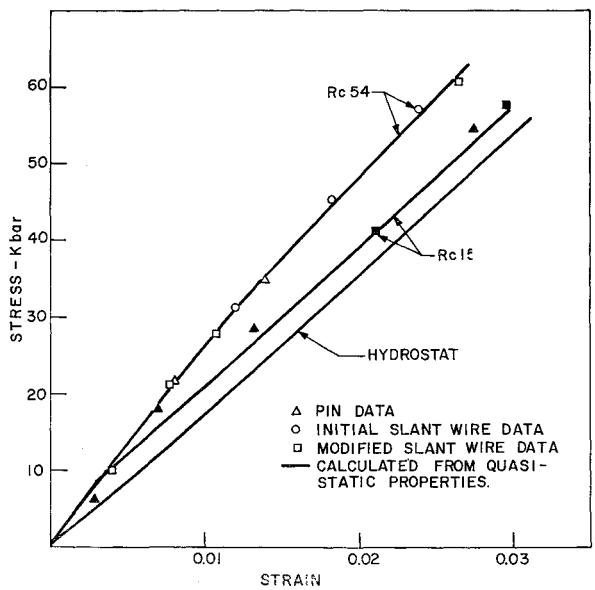

Fig. 6 A comparison of the terminal stress state of R_c54- and R_c15-4340 steel.

†† The terminal stress state is defined as the steady-state stress supported in a region of the material after the wave front has passed through it.

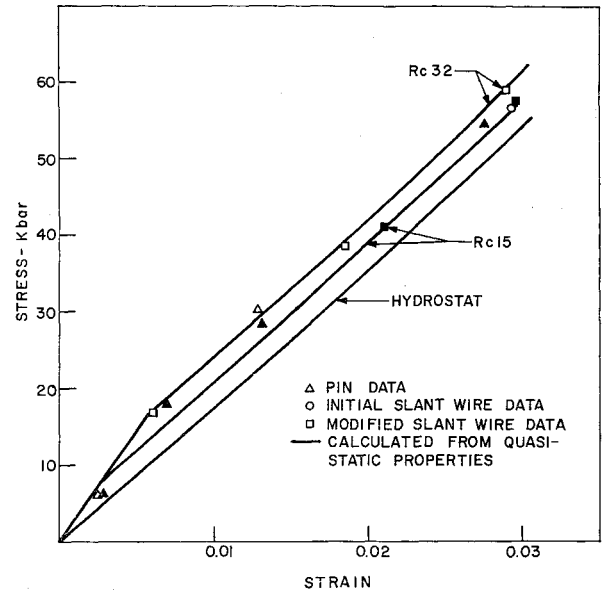

Fig. 7 A comparison of the terminal stress states of R_c32- and R_c15-4340 steel.

average strain rate which is representative of the part of the wave front associated with it. This average reflects the range of strain rates which a given stress increment produces in the material as it propagates through the target and consequently will change as the target thickness is changed. If the dynamic behavior can be represented by a family of curves of constant strain rate,[20–22] where the effect of increase in strain rate is to increase the stress supported by the material for a given value of strain, then the R_c15 experimental curves may be interpreted as follows. Since a steeper wave front is associated with higher strain rates, curves calculated from higher projectile velocity shots must lie further above the hydrostat than those for low velocity shots. The upper parts of all curves, however, will bend back toward the hydrostat through lower strain rates as the peak stress is approached. The last point on the curve, the terminal stress state, represents the condition in the material of almost constant stress and presumably low strain rate. Therefore, it lies in close proximity to the curve calculated from quasi-static data. Unfortunately, the actual stress-strain path to reach this point cannot yet be determined because analysis techniques incorporating strain-rate effects are not available.

An interesting feature of this result is that, if the quasi-static curve is taken for the equation of state of the impacted target, i.e., the projectile velocity remains the same but the target is loaded slowly, the calculated terminal stress is approximately the same as that of the experimentally determined curves. This implies that the terminal stress state is independent of the loading history within the accuracy of the analysis. However, recent electron microscope examinations of shock-loaded metals reveal microstructures that differ considerably from those of specimens loaded slowly to the same final equivalent strain.[23–25] One reason for the close agreement here may be because the effects of microstructural differences may not be sensitively reflected in the one-dimensional strain curves. This is because of the large spherical component of stress present. For example, $\frac{1}{2}\%$ error in stress of the final state of shot 26 could represent a difference of 9% in the flow stress of R_c15 if the hydrostatic stress is known exactly.‡‡ Since $\frac{1}{2}\%$ is the order of the experimental error of this investigation, such a flow

‡‡ For equivalent conditions, this would represent an error of only $2\frac{1}{2}\%$ in R_c54 because of its much greater flow stress.

stress difference would remain undetected. It is evident, however, that the very large increases in flow stress indicated by the large offsets from the quasi-static curve do not persist after the wave front has passed.

The results for R_C32-4340 steel are similar to the R_C15 data with the exception that the maximum offsets from the curve calculated from quasi-static data were only about half the R_C15 curve offsets.

Further details of the differences between the stress-strain curves of R_C15 and R_C54 are in Fig. 6. The work-hardening of the R_C54 steel is reflected by the increasingly large offset from the hydrostat with increasing strain. In contrast, the terminal stress states of R_C15 and R_C32 as plotted in Fig. 7 show that, as the quasi-static tests predict, the only difference is in the larger offset of R_C32-4340 from the hydrostat.

Of secondary interest in these comparisons is the way in which refinements in technique have resulted in better agreement between theory and experiment. The pin shots represent rather gross experimental measurements coupled with an overly simplified analysis, as reflected by the data scatter. The initial slant wire studies were not much better, experimentally, although they did present the opportunity for more exact analysis of the data. The principal difficulty here seems to have been in the way the projectile velocity and tilt were measured. The present experimental technique is accurate enough to give results that are limited by the strain-rate independent condition imposed on the data analysis. There may be many materials, however, such as fully hardened 4340 steel, for which strain-rate effects are small, so that for many applications strain-rate-independent theory adequately describes the propagation of stress waves.

Conclusions

The principal conclusion of this investigation is that the experimentally observed dynamic work-hardening of fully hard 4340 steel is in agreement with its static work-hardening properties. This agreement, along with the observation that strain-rate effects are not large in this steel, suggests that the dynamic stress-strain curve of a material known to be strain-rate insensitive can be accurately predicted from static properties.

A secondary conclusion is that the large increase in flow stress with increase in the strain rate of R_C15- and R_C32-4340 steels is not limited to stress levels around the yield point but persists as long as the strain rate is high. The increase in flow stress is transitory, however, in that, once the wave front is passed and, presumably, the strain rate becomes small, the state of stress in the steel is in agreement with strain-rate-independent theory within experimental error. The validity of this, however, cannot be definitely established until computational techniques incorporating the complicated strain-rate behavior of these materials can be developed.

References

[1] Walsh, J. M. and Christian, R. H., "Equation of state of metals from shock wave measurements," Phys. Rev. **97**, 1544–1556 (1955).

[2] Rice, M. H., McQueen, R. G., and Walsh, J. M., "Compression of solids by strong shock waves," *Solid State Physics*, edited by F. Seitz and D. Turnbull (Academic Press Inc., New York, 1958), Vol. 6, pp. 1–63.

[3] Duvall, G. E., "Properties and applications of shock waves," *Response of Metals to High Velocity Deformation*, edited by P. G. Shewmon and V. F. Zackay (Interscience Publishers, Inc., New York, 1960), pp. 165–203.

[4] Al'tshuler, L. V., Bakonova, A. A., and Trunin, R. F., "Shock adiabats and zero isotherms of seven metals at high pressure," Zh. Eksperim. i Teor. Fiz. **42**, 91–104 (1961); transl. in Soviet Phys. **15**, 65–74 (1962)).

[5] Katz, S., Doran, D. G., and Curran, D. R., "Hugoniot equation of state of aluminum and steel from oblique shock measurement," J. Appl. Phys. **30**, 568–576 (1959).

[6] Hughes, D. S., Gourley, L. E., and Gourley, M. F., "Shock wave compression of iron and bismuth," J. Appl. Phys. **32**, 624–629 (1961).

[7] Taylor, J. W. and Rice, M. H., "Elastic plastic properties of iron," J. Appl. Phys. **34**, 364–371 (1963).

[8] Fowles, G. R., "Shock wave compression of hardened and annealed 2024 aluminum," J. Appl. Phys. **32**, 1475–1487 (1961).

[9] Lundergan, C. D. and Herrmann, W., "Equation of state of 6061-T6 aluminum at low pressures," J. Appl. Phys. **34**, 2046–2053 (1963).

[10] Bancroft, D., Peterson, E. L., and Minshall, S., "Polymorphism of iron at high pressure," J. Appl. Phys. **27**, 291–298 (1956).

[11] Curran, D. R., "Nonhydrodynamic attenuation of shock waves in aluminum," J. Appl. Phys. **34**, 2677–2685 (1963).

[12] Wilkins, M. L., "Calculation of elastic-plastic flow," Lawrence Radiation Lab. Rept. UCRL-7322, Univ. of California (April 1963).

[13] Barker, L. M., Lundergan, C. D., and Herrmann, W., "Dynamic response of aluminum," J. Appl. Phys. **35**, 1203–1212 (1964).

[14] Barker, L. M. and Hollenbach, R. E., "A system for measuring the dynamic properties of materials," Rev. Sci. Instr. **35**, 742–746 (1964).

[15] Wood, D. S., "On longitudinal plane waves of elastic-plastic strain in solids," J. Appl. Mech. **19**, 521–525 (1952).

[16] Morland, L. W., "The propagation of plane irrotational waves through an elasticoplastic medium," Phil. Trans. Roy. Soc. London **A251**, 341–383 (1959).

[17] Barker, L. M., "SWAP-A computer program for shock wave analysis," Sandia Corp. Research Rept. SC-4796(RR) (October 1963).

[18] Bridgman, P. W., "Linear compressions to 30,000 kg/cm^2 including relatively incompressible substances," Proc. Am. Acad. Arts Sci. **77**, 187–233 (1949).

[19] Jones, O. E., Neilson, F. W., and Benedick, W. B., "Dynamic yield behavior of explosively loaded metals determined by a quartz transducer technique," J. Appl. Phys. **33**, 3224–3232 (1962).

[20] Hauser, F. E., Simmons, J. A., and Dorn, J. E., "Strain rate effects in plastic wave propagation," *Response of Metals to High Velocity Deformation*, edited by P. G. Shewmon and V. F. Zackay (Interscience Publishers, Inc., New York, 1960), pp. 93–114.

[21] Karnes, C. H., "Strain-rate effects in cold-worked high purity aluminum," Doctoral Dissertation, Univ. of Texas (1964).

[22] Kolsky, H. and Douch, L. S., "Experimental studies in plastic wave propagation," J. Mech. Phys. Solids **10**, 195–223 (1962).

[23] Leslie, W. C., Hornbogen, E., and Dieter, G. E., "Structure of shock hardened iron," J. Iron Steel Inst. (London) **200**, 622–633 (1962).

[24] Johari, O. M. and Thomas, G., "Substructures in plastically deformed copper," Lawrence Radiation Lab. Rept. UCRL-10932 Rev., Univ. of California (October 1963).

[25] Estill, W. B. and Mullendore, A. W., private communication, Sandia Corp. (1963).